Surface Modification of $\alpha-Fe_2O_3$ Nanoparticles to Develop as Intrinsic Photoluminescent Probe and Unprecedented Photocatalyst

Monalisa Pal, Rupali Rakshit, Madhuri Mandal, and Kalyan Mandal

S. N. Bose National Center for Basic Sciences, Kolkata 700098, India

Herein, we demonstrate the emergence of intrinsic multicolor fluorescence in $\alpha-Fe_2O_3$ nanoparticles (NPs) from blue, cyan, to green, upon functionalization and further surface modification with a small organic ligand, Na–tartrate. Furthermore, we have found an excellent photocatalytic property of the functionalized $\alpha-Fe_2O_3$ NPs in the decoloration of a model water contaminant. Detailed characterization of $\alpha-Fe_2O_3$ NPs before and after functionalization were carried out by X-ray diffraction and transmission electron microscopy. Proper investigation through UV-visible absorption and photoluminescence study along with theoretical support from literature reveals that ligand-to-metal charge transfer from tartrate ligand to lowest unoccupied energy level of Fe^{3+} of the NPs and d–d transitions centered over Fe^{3+} ions in the NPs play the key role in the generation of multiple fluorescence from the ligand functionalized $\alpha-Fe_2O_3$ NPs. Vibrating sample magnetometry measurements exhibit magnetic behavior of Fe_2O_3 NPs changed considerably after surface modification. We believe that the developed ferromagnetic, multicolor fluorescent $\alpha-Fe_2O_3$ NPs would pioneer new opportunities toward diverse applications.

Index Terms—**Intrinsic fluorescence, magnetic nanoparticles (MNPs), photocatalysis, surface modification.**

I. Introduction

METAL oxide nanoparticles (NPs) have attracted substantial interest because of their unique optical, magnetic, electronic, or catalytic properties in recent years. Combination of two or more properties within a single entity in nanoscale to develop multifunctional nanoprobe for their advanced application in several biological and technological field has been a key topic in the past decade. Intersection of nanotechnology with biology has resulted in a progressive development of a new emerging research area called nanobiotechnology. Properly functionalized magnetic nanoparticles (MNPs) possess several advantages that give rise to many exciting opportunities in the field of biomedical applications, such as magnetic tweezers, separation of proteins [1] and DNA molecules [2] and therapeutic applications, including ac magnetic field-assisted hyperthermia [3]. Moreover, MNPs can be manipulated by external field, which facilitates targeted delivery of drugs and radioactive isotopes for chemotherapy and radiotherapy and in noninvasive diagnosis as contrast enhancement agent in magnetic resonance imaging (MRI) [4] along with fluorescence imaging [5]. The size tunability of MNPs from few nanometers to tens of nanometers enhances their interaction possibility with different biological entities. Very recently, significant attention has also been directed toward the development of MNPs as sustainable nanocatalyst for specific chemical transformations having both economic and environmental significance, considering their efficient activity, low cost, simple preparation method, high stability, and controlled separation by external magnetic field [6]. So far different research groups have prepared fluorescent MNPs either by molecular functionalization with fluorescent dyes or polymers or forming nanocomposites with quantum dots [7], [8]. Insufficient photostability of fluorescent dyes and inherent toxicity of quantum dots (QDs) impose serious limitation to their bio-imaging applications [9]. Therefore, for improvement of the efficiency of the MNPs for biomedical applications, the development of biocompatible MNPs having intrinsic fluorescence property and photo stability, is highly required. Among the MNPs, Fe_2O_3 nanomaterials have attracted increasing attention because of their inherent environmentally benign character and outstanding thermal stability in practical applications, such as magnetic storage, targeted drug delivery [10], gas sensing, as photoanodes for photoassisted electrolysis and catalysis [11]–[14]. However, development of intrinsic fluorescence from surface functionalized $\alpha-Fe_2O_3$ NPs is sparse in literature. However, despite recent advancement, aqueous phase insolubility, and absence of any inherent optical properties of the NPs restrict their direct biomedical applications. Thus, fabrication of appropriately surface modified $\alpha-Fe_2O_3$ NPs to explore the diverse biological and technological applicability is highly desirable.

Herein, we report the development of $\alpha-Fe_2O_3$ NPs as a multifunctional nanoprobe having intrinsic multicolor fluorescence, ferromagnetism, and novel photocatalytic activity. We have synthesized $\sim$35 nm $\alpha-Fe_2O_3$ NPs following a wet chemical method previously reported by Sun *et al.* [15], with slight modification. Using the reactivity of tartrate ligands, we have solubilized the as-prepared NPs into aqueous environment. Further surface modification of water dispersed tartrate functionalized $\alpha-Fe_2O_3$ NPs has given rise to the emergence of multicolor fluorescence (starting from blue, cyan, to green). Origin of this novel multicolor fluorescence property, can be easily explained with ligand field theory. It has been found

that the ligand-to-metal charge transfer (LMCT) from tartrate ligand to lowest unoccupied energy levels of Fe^{3+} metal ions in the NPs and d–d transitions play the key role. Finally, we intended to utilize the photo excitation (UV-vis) of the functionalized $\alpha-Fe_2O_3$ NPs in catalysis. It has been found that, the functionalized $\alpha-Fe_2O_3$ NPs exhibit unprecedented photocatalytic property in the degradation of methylene blue (MB), a commonly used organic dye in textile industries and a model water contaminant.

II. Experimental Section

1) Material Used: Fe(III)acetylacetonate, oleylamine, and MB were obtained from Sigma-Aldrich. Diphenyl ether, oleic acid, and cetyl alcohol were received from Loba Chemie. Tartaric acid and sodium hydroxide (NaOH) were purchased from Merck. All the reagents are of analytical grade and used without further purification.

2) Synthesis Procedure and Functionalization of $\alpha-Fe_2O_3$ NPs: $\alpha-Fe_2O_3$ NPs were synthesized by template free wet chemical process following a previous report with some modification [15], involving the high-temperature (260 °C) reflux of $Fe(acac)_3$ in di-phenyl ether in the presence of oleic acid, oleylamine, and cetyl alcohol, followed by annealing at 550 °C. As-prepared $\alpha-Fe_2O_3$ NPs were cyclomixed with 0.5 M Na–tartrate solution (prepared in Milli-Q water and pH of the solution were made ∼7) for 12 h at room temperature. The nonfunctionalized larger $\alpha-Fe_2O_3$ NPs were filtered out with a syringe filter of 0.22 μm diameter. The as-obtained colorless filtrate was tartrate functionalized $\alpha-Fe_2O_3$ NPs, called T-Fe_2O_3 NPs. To induce the multicolor fluorescence property and enhance the intensity, T-Fe_2O_3 NPs were heated at about 70 °C for 8 h under extensive stirring condition maintaining the pH of the solution at ∼12 with drop wise addition of NaOH solution. To prepare the solid powdered samples required for magnetic study vibrating sample magnetometry (VSM), we dialyzed functionalized Fe_2O_3 NPs solution (to remove excess ligands) and lyophilized followed by drying over a water bath.

3) Characterization Techniques: X-ray diffraction (XRD) patterns were obtained by employing a scanning rate of 0.02° s^{-1} in the 2θ range from 20° to 80° by Rigaku miniflex II diffractometer equipped with Cu– K_α radiation (at 40 mA and 40 kV).

For transmission electron microscopy (TEM) study samples were prepared by drop casting of the dispersed NPs on a 300-mesh carbon coated copper grid and dried overnight in air. Particle size was determined from TEM micrographs and elemental analysis was performed from Energy-dispersive X-ray spectroscopy (EDAX) spectrum recorded by a FEI Tecnai TF-20 field-emission high-resolution transmission electron microscope operating at 200 kV.

UV-vis absorbance spectra of the T-Fe_2O_3 NPs were recorded with a Shimadzu Model UV-2600 spectrophotometer using a quartz cuvette of 1 cm path length. Steady-state fluorescence emission and excitation spectra of T-Fe_2O_3 NPs were recorded on Horiba Jobin Yvon Model Fluorolog fluorimeter.

Magnetic study was carried out in a Lake Shore VSM equipped with an electromagnet, capable of generating field of up to 1.6 T at 300 K.

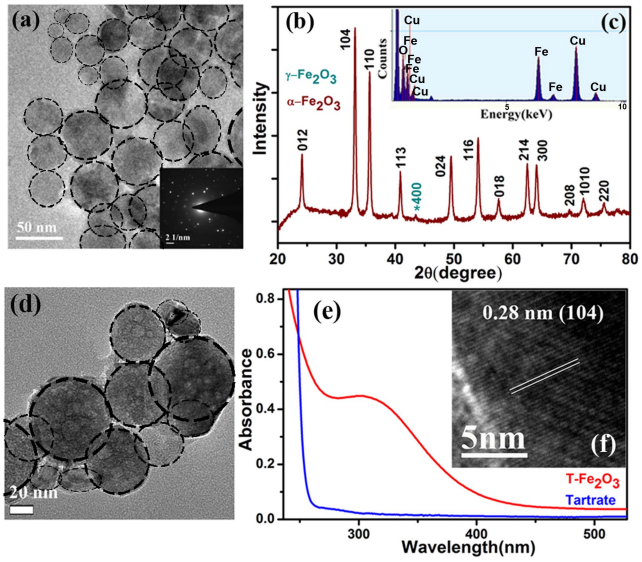

Fig. 1. (a) TEM image of the as-prepared bare $\alpha-Fe_2O_3$ NPs. In the inset SAED pattern of $\alpha-Fe_2O_3$ NPs indicates high crystallinity. (b) XRD pattern of as-prepared $\alpha-Fe_2O_3$ NPs. All diffraction peaks in the figure are perfectly indexed in the literature to the rhombohedral corundum structure of $\alpha-Fe_2O_3$ NPs. (c) EDAX spectrum of the NPs indicating the presence of both Fe and O. (d) TEM image of the tartrate functionalized $\alpha-Fe_2O_3$NPs. (e) UV-vis absorption spectrum for T-Fe_2O_3 NPs and Na–tartrate at pH ∼ 7. (f) HR-TEM image of T-Fe_2O_3NPs indicates high crystallinity and shows lattice fringes.

For the study of photocatalysis, we used 8 W UV lamp as UV light source from Philips. Aqueous solution of MB and T-Fe_2O_3 NPs were homogeneously mixed for 1 h in a quartz cuvette in the dark maintaining the pH of the solution ∼3. Then, the cuvette was placed ∼2 cm apart from the light source and the absorbance of MB in the reaction mixture was measured time to time by the UV-vis spectrophotometer.

III. Results and Discussion

A. Nanoparticle Characterization

TEM study was carried out to have an idea about the size and morphology of the as prepared NPs. TEM image of $\alpha-Fe_2O_3$ NPs, as shown in Fig. 1(a), demonstrates that average size of the particles were found to be ∼35 nm. Moreover, in the inset of Fig. 1(a), the selected area electron diffraction (SAED) pattern indicates high crystallinity of the as prepared $\alpha-Fe_2O_3$ NPs. XRD pattern of as obtained product, as shown in Fig. 1(b), exactly matches with the α phase of Fe_2O_3 (JCPDS, file no. 17-0536). A peak corresponding to (400) plane of $\gamma-Fe_2O_3$ indicates the presence of very small amount of impurity within the NPs. EDAX spectrum of the NPs, as shown in Fig. 1(c), confirms the presence of both Fe and O.

To solubilize $\alpha-Fe_2O_3$ NPs in aqueous medium, we functionalized them with biocompatible organic ligand, Na–tartrate. After surface functionalization size of the particles remained almost unchanged, as evident from Fig. 1(d). The high-resolution transmission electron microscopy (HR-TEM) image of T-Fe_2O_3 NPs [as shown in Fig. 1(f)] clearly indicates high crystalline nature of the NPs. The calculated interplanar distance between the fringes has been found to be 0.28 nm

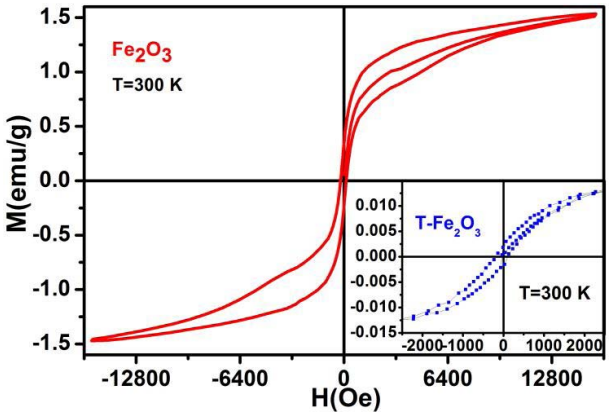

Fig. 2. Magnetization versus applied magnetic field plot for the as-prepared bare $\alpha-Fe_2O_3$ NPs. In the inset hysteresis loop of T-Fe_2O_3 NPs indicates ferromagnetic nature.

corresponding to (104) plane of the crystal lattice. UV-vis absorbance spectrum, as shown in Fig. 1(e), consists of a broadband near 320 nm.

B. Magnetic Properties

Fig. 2 shows the magnetic study of both bare and T-Fe_2O_3 NPs (inset) at room temperature. It is noticeable that the shape of the hysteresis loop is constricted. Constricted loops are typically observed in materials with a mixture of a soft and hard magnetic phase. Thus, at room temperature the observed response could be due to combination of α and very small amount of γ phases of Fe_2O_3 (as evident from the XRD). The γ phase is a soft phase with higher moment, whereas the α phase has the higher coercivity and lower moment. Combination of these two magnetic properties leads to a constricted hysteresis loop. The coercivity of as prepared sample is found to be 174 Oe and the magnetization curve dose not saturate up to the maximum applied magnetic field of 1.6 T. After surface modification, the magnetic behavior of Fe_2O_3 NPs. (i.e., in case of T-Fe_2O_3) is converted to typical ferromagnetic nature with slight decrease in coercivity (145 Oe) and saturation magnetization. The change in magnetic behavior upon surface modification can be explained by ligand field theory [16]. Tartrate ligand, containing both the σ-donor ($-OH^-$) and π-donor ($-COO^-$) favors the quenching of magnetic moments of Fe^{+3} ions over the surface of T-Fe_2O_3NPs and subsequently reduces its spin–orbit coupling, causing decrease in magnetocrystalline anisotropy, which results in decrease in coercivity [17], [18] of T-Fe_2O_3 NPs as compared with bare one. Further mathematically, as stated in Stoner–Wohlfarth theory, the magnetocrystalline anisotropy energy E_A of a single-domain particle can be approximated as

$$E_A = KV \sin^2\theta \tag{1}$$

where K is the magnetocrystalline anisotropy constant, V is the volume of a NP, and θ is the angle between magnetization direction and easy axis of NP. Since K is determined by the strength of spin–orbit coupling, reduced spin–orbit coupling results in a decrease in magnetocrystalline anisotropy of the NP system; and therefore, the coercivity of the system.

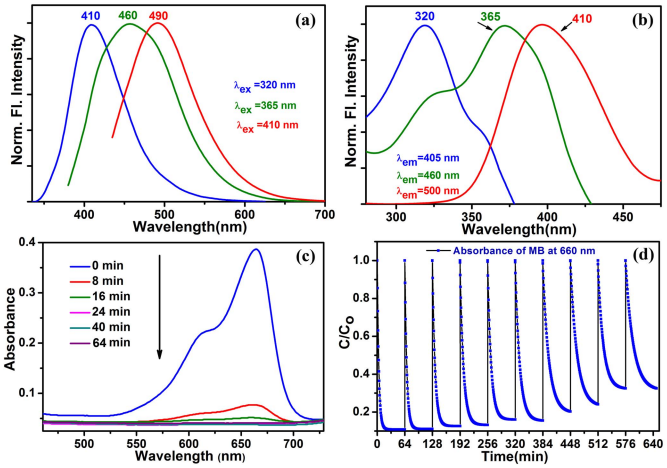

Fig. 3. (a) Normalized steady-state fluorescence emission spectra collected from T-Fe_2O_3 NPs with three different excitation wavelengths of 320, 365, and 410 nm. (b) Fluorescence excitation spectra of T-Fe_2O_3 NPs at different emission maximum of 405, 460, and 500 nm. (c) UV-vis spectral changes of aqueous solution of MB in presence of T-Fe_2O_3 NPs with time, under UV irradiation. (d) Plot of relative concentration of MB monitored at 660 nm versus time for consecutive 10 Hz, showing reusability of T-Fe_2O_3 in MB degradation under UV light.

C. Fluorescence Properties

Fig. 3(a) shows normalized steady-state fluorescence emission spectra as obtained from T-Fe_2O_3 NPs. Upon excitation at wavelength of 320 and 365 nm, the solution gave rise to intense fluorescence peak at 410 and 460 nm, respectively. Further surface modification of the as obtained solution, involving heat and pH treatment, gave rise to fluorescence at 490 nm upon excitation at 410 nm. The other expected bands at around 365 and 410 nm were not observed in the absorption spectrum presumably because the band had been masked by the more intense 320 nm absorption, however, was distinctly visible in the excitation spectrum, as shown in Fig. 3(b). The mystery behind the generation of intrinsic fluorescence can be solved by ligand field theory [19]. Peaks arising at 410 nm can be attributed to LMCT involving highest occupied molecular orbital of tartrate ligand and lowest unoccupied molecular orbital centered over metal ion Fe^{+3}. The other fluorescence peaks at 460 and 490 nm upon excitation at 365 and 410 nm can be attributed to ${}^6A_{1g} \rightarrow {}^4T_{1g}$ and ${}^6A_{1g} \rightarrow {}^4T_{2g}$ transitions, respectively, due to the crystal field splitting of a FeO_6 octahedron with O_h symmetry as the first approximation. Both are actually dipole and spin forbidden transitions; however, they can have considerable strengths due to the relaxation of selection rules by lattice distortion and spin–orbit coupling as discussed in other $Fe^{3+}(3d^5)$ materials [20].

D. Photocatalytic Properties

Considering the recent explosive growth of nanocatalyst to accelerate the reaction rate, we sought to develop more efficient photocatalyst for waste water treatment, utilizing the strong absorbance of the functionalized $\alpha-Fe_2O_3$ NPs in the UV-vis region. T-Fe_2O_3 NPs showed unprecedented photocatalysis of MB, a commonly used dye in textile industries upon UV light irradiation, as shown in Fig. 3(c). We have

found that photodegradation of MB in presence of T-Fe_2O_3 NPs takes place exponentially with time following first-order rate equation with a kinetic rate constant (k) of 27.55×10^{-2} min^{-1}. We also checked the reusability of the catalyst, after every 64 min we added same dose of MB into the reaction mixture up to 10 dose, keeping the catalyst concentration fixed (without addition of extra catalyst after the first cycle), MB decomposition rates of different cycles were measured by monitoring the decrease of MB absorbance at 660 nm using UV-vis spectroscopy. Fig. 3(d) shows the plots of relative concentration of MB versus time, up to consecutive 10 Hz, revealing the reusability of T-Fe_2O_3 NPs catalyst with almost unchanged degradation rate. We propose that photodegradation procedure may follow radical pathway involving reactive oxygen species [21], [22], as recently reported by Giri *et al.* [23] in case of ligand functionalized Mn_3O_4 NPs.

IV. Conclusion

In conclusion, surface modified $\alpha-Fe_2O_3$ NPs have been prepared by a very easy ligand functionalization process. The newly developed multifunctional $\alpha-Fe_2O_3$ NPs show simultaneously intrinsic multiple fluorescence covering a broad range of UV-vis region from blue, cyan, to green, inherent ferromagnetism and excellent photocatalytic properties. We have successfully explained our interesting experimental findings with previously reported theory. We hope that our newly developed magnetofluorescent $\alpha-Fe_2O_3$ NPs will be a promising candidate for several biological and technological applications, such as bioimaging, drug delivery, and wastewater treatment. Moreover, a logical extension of this paper would be the investigation of the influence of external magnetic field on fluorescence spectra and the effect of particle size on both magnetic and fluorescence property of the materials.

Acknowledgment

This work was supported in part by CSIR and in part by SNBNCBS, Government of India.

References

[1] M. Kuhara, H. Takeyama, T. Tanaka, and T. Matsunaga, "Magnetic cell separation using antibody binding with protein a expressed on bacterial magnetic particles," *Anal. Chem.*, vol. 76, pp. 6207–6213, Oct. 2004.

[2] B. Yoza, A. Arakaki, K. Maruyama, H. Takeyama, and T. Matsunaga, "Fully automated DNA extraction from blood using magnetic particles modified with a hyperbranched polyamidoamine dendrimer," *J. Biosci. Bioeng.*, vol. 95, no. 1, pp. 21–26, 2003.

[3] M. Johannsen *et al.*, "Clinical hyperthermia of prostate cancer using magnetic nanoparticles: Presentation of a new interstitial technique," *Int. J. Hyperthermia*, vol. 21, no. 7, pp. 637–647, Nov. 2005.

[4] H. B. Na, I. C. Song, and T. Hyeon, "Inorganic nanoparticles for MRI contrast agents," *Adv. Mater.*, vol. 21, no. 21, pp. 2133–2148, Mar. 2009.

[5] J. Yang *et al.*, "Fluorescent magnetic nanohybrids as multimodal imaging agents for human epithelial cancer detection," *Biomaterials*, vol. 29, no. 16, pp. 2548–2555, Jun. 2008.

[6] M. B. Gawande, P. S. Branco, and R. S. Varma, "Nano-magnetite (Fe_3O_4) as a support for recyclable catalysts in the development of sustainable methodologies," *Chem. Soc. Rev.*, vol. 42, no. 8, pp. 3371–3393, Feb. 2013.

[7] H. Kim, M. Achermann, L. P. Balet, J. A. Hollingsworth, and V. I. Klimov, "Synthesis and characterization of Co/CdSe core/shell nanocomposites: Bifunctional magnetic-optical nanocrystals," *J. Am. Chem. Soc.*, vol. 127, no. 2, pp. 544–546, 2005.

[8] J. Gao, W. Zhang, P. Huang, B. Zhang, X. Zhang, and B. Xu, "Intracellular spatial control of fluorescent magnetic nanoparticles," *J. Am. Chem. Soc.*, vol. 130, no. 12, pp. 3710–3711, Mar. 2008.

[9] U. Resch-Genger, M. Grabolle, S. Cavaliere-Jaricot, R. Nitschke, and T. Nann, "Quantum dots versus organic dyes as fluorescent labels," *Nature Methods*, vol. 5, pp. 763–775, Aug. 2008.

[10] A. Kumar, P. K. Jena, S. Behera, R. F. Lockey, S. Mohapatra, and S. Mohapatra, "Multifunctional magnetic nanoparticles for targeted delivery," *Nanomed., Nanotechnol., Biol. Med.*, vol. 6, no. 1, pp. 64–69, Feb. 2010.

[11] W. Weiss, D. Zscherpel, and R. Schlögl, "On the nature of the active site for the ethylbenzene dehydrogenation over iron oxide catalysts," *Catalysis Lett.*, vol. 52, pp. 215–220, Jul. 1998.

[12] T. Ohmori, H. Takahashi, H. Mametsuka, and E. Suzuki, "Photocatalytic oxygen evolution on-Fe_2O_3 films using Fe3+ ion as a sacrificial oxidizing agent," *Phys. Chem. Chem. Phys.*, vol. 2, pp. 3519–3522, Jul. 2000.

[13] E. Comini, V. Guidi, C. Frigeri, I. Riccò, and G. Sberveglieri, "CO sensing properties of titanium and iron oxide nanosized thin films," *Sens. Actuators B, Chem.*, vol. 77, nos. 1–2, pp. 16–21, Jun. 2001.

[14] Z. Li *et al.*, "Dehydrogenation improvement of $LiAlH_4$ catalyzed by Fe_2O_3 and Co_2O_3 nanoparticles," *J. Phys. Chem. C*, vol. 117, no. 36, pp. 18343–18352, Aug. 2013.

[15] S. Sun *et al.*, "Monodisperse MFe_2O_4 (M = Fe, Co, Mn) nanoparticles," *J. Am. Chem. Soc.*, vol. 126, no. 1, pp. 273–279, Dec. 2003.

[16] P. Crespo *et al.*, "Magnetism in nanoparticles: Tuning properties with coatings," *J. Phys., Condens. Matter*, vol. 25, no. 48, p. 484006, Nov. 2013.

[17] C. R. Vestal and Z. J. Zhang, "Effects of surface coordination chemistry on the magnetic properties of $MnFe_2O_4$ spinel ferrite nanoparticles," *J. Am. Chem. Soc.*, vol. 125, no. 32, pp. 9828–9833, Jul. 2003.

[18] R. Rakshit, M. Mandal, M. Pal, and K. Mandal, "Tuning of magnetic properties of $CoFe_2O_4$ nanoparticles through charge transfer effect," *Appl. Phys. Lett.*, vol. 104, no. 9, pp. 092412-1–092412-4, Mar. 2014.

[19] A. Giri *et al.*, "Emergence of multicolor photoluminescence in $La_{0.67}Sr_{0.33}MnO_3$ nanoparticles," *J. Phys. Chem. C*, vol. 116, no. 48, pp. 25623–25629, Nov. 2012.

[20] J. H. Jung, M. Matsubara, T. Arima, J. P. He, Y. Kaneko, and Y. Tokura, "Optical magnetoelectric effect in the polar $GaFeO_3$ ferrimagnet," *Phys. Rev. Lett.*, vol. 93, no. 3, p. 037403, Jul. 2004.

[21] A. Giri *et al.*, "Unprecedented catalytic activity of Mn_3O_4 nanoparticles: Potential lead of a sustainable therapeutic agent for hyperbilirubinemia," *RSC Adv.*, vol. 4, no. 10, pp. 5075–5079, Dec. 2014.

[22] M. Pal, R. Rakshit, and K. Mandal, "Surface modification of $MnFe_2O_4$ nanoparticles to impart intrinsic multiple fluorescence and novel photocatalytic properties," *ACS Appl. Mater. Inter.*, vol. 6, no. 7, pp. 4903–4910, Mar. 2014.

[23] A. Giri *et al.*, "Rational surface modification of Mn_3O_4 nanoparticles to Induce multiple photoluminescence and room temperature ferromagnetism," *J. Mater. Chem. C*, vol. 1, no. 9, pp. 1885–1895, Jan. 2013.